X-ray Interferometers Based on Refractive Optics

A. Snigirev[a], I. Snigireva[a], V. Kohn[b], S. Kuznetsov[c], and V. Yunkin[c]

[a]*ESRF, B.P. 220, 38043 Grenoble, France*
[b]*Russian Research Center "Kurchatov Institute", 123182 Moscow, Russia*
[c]*IMT RAN, 142432 Chernogolovka, Moscow region, Russia*

Abstract. A novel type of hard x-ray interferometers employing compound refractive lenses is proposed. One such interferometer is a bilens system with two parallel arrays of planar refractive lenses. Under coherent illumination the bilens generates two diffraction-limited mutually coherent beams. Slightly overlapping these beams produces an interference pattern with a fringe spacing ranging from tens of nanometers to tens of micrometers. This simple way to create an x-ray standing wave in paraxial geometry opens up the opportunity to develop new x-ray interferometry techniques to study natural and advanced man-made nanoscale materials, such as self-organized biosystems, photonic and colloidal crystals, and nanoelectronics materials.

Keywords: Interferometer, refractive optics, bilens, coherence
PACS: 41.50.+h; 07.85.Qe; 61.05.cp

INTRODUCTION

Following the successful development and application of refractive optics for high-energy x-rays [1-4], we propose a new type of interferometry for high-energy x-rays. One such interferometer is similar to the model of the Billet split lens in classical optics [5]. The schematic diagram of our interferometer is shown in Fig. 1. It consists of two identical, parallel planar compound refractive lenses separated transversally by a distance d. Each lens focuses the beam at a distance $z_f = F/(1 - F/z_0)$, where $F = R/2N\delta$ is the lens focal length, z_0 is the source-to-bilens distance, R is the radius of curvature of one parabolic surface, N is the number of double concave elements in the lens, and δ is the decrement of refraction index $n = 1 - \delta + i\beta$. Similar to the double-slit scheme, the split distance d of the bilens should be smaller than the spatial coherence length of the incoming beam defined as $l_{coh} = \lambda z_0/S$, where S is the effective source size (FWHM). As a consequence, each lens is illuminated coherently, and therefore it generates a coherent, diffraction-limited focal spot of size $\sigma = \lambda z_f/A_{eff}$, where A_{eff} is the absorption-limited effective aperture of the lens [1]. At a distance $z_1 > z_f\, d/A_{eff}$, the cones diverging from these secondary sources overlap, and in this region of superposition, interference occurs. The fringe spacing is given by $\Lambda = \lambda z_1/d$. It should be noted that this pattern has a variable period ranging from tens of nanometers to tens of micrometers, depending on the distance z_1. In order to extend the field of view, the interferometer can be evolved into a multi-lens system where more than two parallel arrays can be used [6].

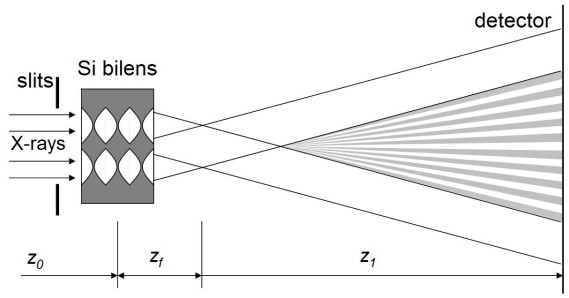

FIGURE 1. Schematic view of bilens interferometer.

The 10th International Conference on X-ray Microscopy
AIP Conf. Proc. 1365, 285-288 (2011); doi: 10.1063/1.3625360

EXPERIMENT

The planar bilenses were manufactured by a microfabrication process consisting of two main steps: pattern generation of a hard mask on the silicon surface, and pattern transfer into the silicon. By optimizing the lens design and the manufacturing process we were able to produce lenses with rigorously vertical sidewalls of up to 70 μm in depth. The length and aperture of each single, double-concave individual lens are 102 and 50 μm, respectively. The radius of curvature of one parabolic surface is R = 6.25 μm, and the minimum thickness of the material between the apexes of two parabolic surfaces is 2 μm. The measured roughness of the lens surface is of the order of 20 nm. The split distance between lenses is d = 60 μm. A magnified SEM image of the bilens interferometer is shown in Fig. 2(a). In order to obtain reasonably short focal distances at higher energies five bilens interferometers were manufactured on the same Si chip. They differ in the number of individual parabolic lenses, and as result they have different focal distances and cover a range of x-ray energies from 10 to 50 keV (Fig. 2(b)). Table 1 summarizes the main parameters of the bilens sets.

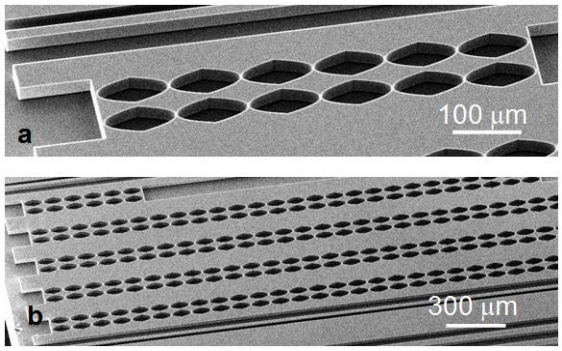

FIGURE 2. (a) Scanning electron micrograph of a single Si bilens and (b) general view with five bilenses.

The experimental tests of the bilens interferometer were carried out at the ESRF beamline ID06. A Si-111 double-crystal monochromator was used to select x-ray energy in the range of 10-20 keV. The Si bilens system was mounted at a distance z_0 = 54.16 m from the source. Interference patterns were recorded with a high-resolution x-ray CCD camera (Sensicam) with a spatial resolution of about 1.3 μm (0.645-μm pixel size).

To record the interference pattern in the far field, the CCD camera was placed a distance z_f+z_1 = 3.94 m from the bilens. The typical exposure time was 5-10 seconds. As the spatial coherence is much higher vertically, all measurements of interference patterns were made vertically. The observed interference pattern and intensity variation are shown in Fig. 3. The measured fringe spacing was Λ = 6.25 μm, in very good agreement with calculations. The quality of the fringes can be described quantitatively using the visibility V:

$$V = \frac{I_{\max} - I_{\min}}{I_{\max} + I_{\min}} = \exp\left[-\frac{\pi^2}{4 \ln 2} \left(\frac{S(z_f + z_1)}{\Lambda z_0} \right)^2 \right] \quad . \tag{1}$$

Here I_{max} and I_{min} are the irradiances corresponding to the maximum and adjacent minimum in the fringe system. As for the Young double slit, the visibility is a function of the source size and can be used as a measure of the degree of spatial coherence or of effective source size.

TABLE 1. Main design parameters of the bilenses (all parameters are calculated for an x-ray energy of 12 keV)

Set	Number of lenses	Total lens length, μm	Focal length, cm	Diffraction limited resolution, nm	Effect. aperture, μm
1	6	620	14.9	270	38
2	26	2660	3.5	130	18.4
3	58	5924	1.67	90	12.3
4	104	10616	1.05	70	10
5*	162	16532	-	-	-

* bilens #5 is not optimal for 12 keV, while it is designed for higher energies > 20 keV

The measured value of the visibility was about 38% (Fig. 3(a)). From this it follows that the effective source size in the vertical direction was 45 ±5 μm (FWHM), which coincides with data found by the interferometric technique [7]. For all tested bilenses the recorded interference patterns showed the same visibility, around 38 ±2%, as expected from Eq. (1), as $z_f << z_1$. Considering that the lens effective aperture A_{eff} changes by a factor of 5 and that the number of concave surfaces changes by factor of 27 from set 1 to set 5, we conclude that the lens quality is excellent. This was verified by measuring the focusing properties of individual lenses from bilens set #2 by the knife-edge scanning technique. A focus of 130 nm (FWHM) was measured, showing the theoretical diffraction limit for E = 12 keV.

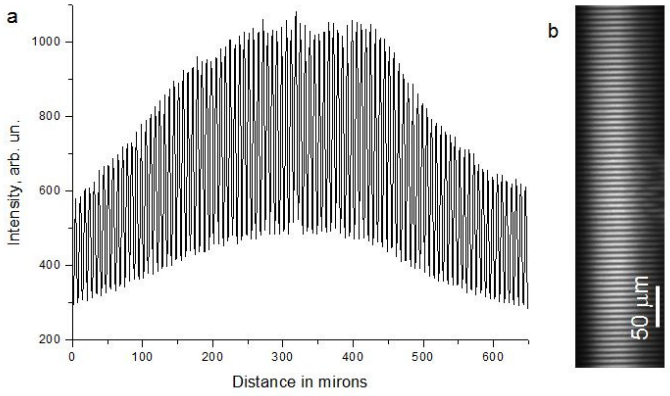

FIGURE 3. The intensity variation (a) obtained through the center of the interference pattern (b) generated by second bilens at 12 keV.

To resolve the nanometer-scale interference fringes in the near field we apply scanning and imaging (Fig. 4) techniques using a 0.5-μm-thick Ta grid with a 400-nm periodicity (200-nm slit and 200-nm bar) behind the bilens. In the scanning mode the intensity modulations are measured with a PIN-diode by moving the grid across the fringes generated by the bilens. The Ta grid was placed 270 mm from the bilens, where the pitches of the grid and interference pattern coincided; the vertical scan of the grid in the vertical direction is shown in Fig. 4(b). To visualize a nano-pattern we applied a moiré imaging technique in which two periodical patterns with slightly different pitch sizes interfere. Moving the Ta grid along the bilens optical axis, we probed the pitch of interference pattern. At a distance of 270 mm the grid and the interference pattern pitch coincide, and moiré fringes are absent (Fig. 4(c)). Depending on the grid displacement from this position, the moiré pattern changes from 2 to 5 fringes with periodicity from 8 μm to 4 μm (Figs. 4(c)-4(e)). We emphasize that the change in the number of fringes from 4 (Fig 2(d)) to 5 (Fig 2(e)) corresponds to a 5-nm increase of the bilens interference pitch size and 3-mm longitudinal grid shift, demonstrating the extreme precision of the technique. A coherent moiré imaging or radiography technique using bilens is a straightforward application. The evident advantage of moiré radiography over the direct measurement of the interference fringes is that it greatly reduces the requirements on detector resolution while still offering submicron and nanometer resolution.

In order to address the question of the smallest period of x-ray standing waves that can be generated by the bilens interferometer, let us consider the case of a fully coherent point source. In this case the incident wave can be treated as a plane wave. We restrict ourselves by the thin lens approximation, where the compound lens consisting of N double-concave elements is equivalent to a single lens with an N times smaller radius of curvature. In the following we choose the lens length equal to $L = F/4$, the focal length as $F = R/2\delta$, and the lens geometrical aperture $A = 2(RL)^{1/2} = R(2\delta)^{-1/2}$. When the split distance d is equal to the lens geometrical aperture, the superposition of the two beams starts at distance $z_1 = F$.

The minimum fringe spacing is $\Lambda = \lambda F/A = \lambda/(2\delta)^{1/2}$. As δ is proportional to λ^2, the fringe spacing is nearly independent of the x-ray energy. From this it would seem that high-Z materials are favorable; for example, for the gold bilens we calculate $\Lambda = 16$ nm. However, the absorption in high-Z materials drastically reduces the lens effective aperture. In the case of a gold bilens the submicron aperture makes the use of such materials unfeasible. Taking the attenuation inside the lens into account, the minimum fringe separation can be achieved when the geometrical aperture and split distance are smaller than the lens effective aperture $A < A_{\text{eff}}$, i.e., $R(2\delta)^{-1/2} < 0.47(\lambda R/\beta)^{1/2}$ or $R < 0.44\,\lambda\delta/\beta$. In this case, the radius of curvature strongly depends on the x-ray energy and lens material. The best performance is therefore expected for high-density low-Z materials such as diamond, silicon, and beryllium. So for silicon we have $\Lambda = 40$ nm,

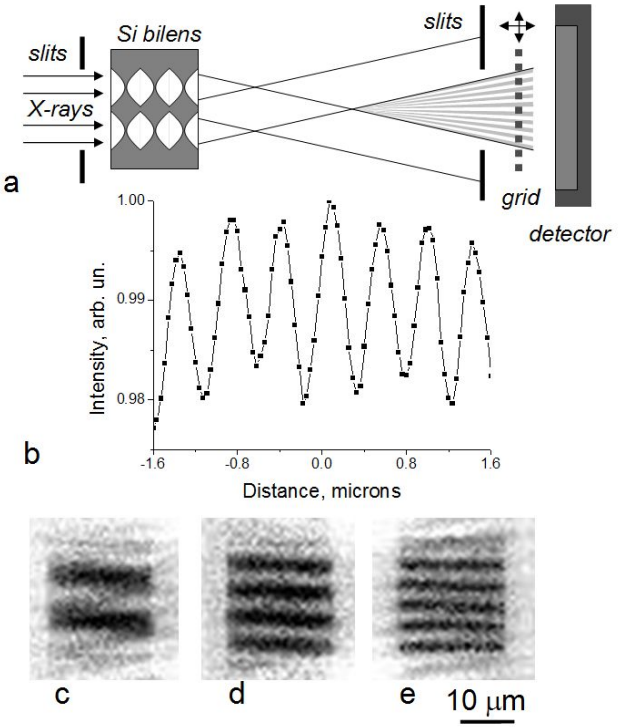

FIGURE 4. (a) Layout for interference recording in the near field. (b) Intensity modulation by scanning Ta grid. X-ray moiré patterns taken at distances (c) 280 mm, (d) 288 mm, (e) 291 mm.

and an aperture $A > 20$ μm can be used above 50 keV. The best material is diamond for which $\Lambda = 33$ nm, and $A > 20$ μm is at $E > 12$ keV. The beryllium bilens can generate fringes $\Lambda = 48$ nm in a broad energy range, and the largest aperture $A = 102$ μm is at $E = 20$ keV.

CONCLUSION

We have demonstrated a new and simple way to generate an x-ray periodic interference field such as a standing wave with variable period ranging from tens of nanometers to tens of micrometers. The proposed interferometer thus occupies the place between crystal and grating interferometers. The silicon bilens can generate standing waves with a 40-nm period above 50 keV. If diamond lenses were employed, then we could expect the smallest pitch to be 30 nm at energies E > 12 keV. Contrary to Bonse-Hart interferometers and x-ray standing wave techniques, the bilens interferometer generates an interference pattern without the requirement of additional optics like crystals or multilayers. The interference occurs in air at a reasonable distance from the device itself, allowing great flexibility in sample size and environment.

Such coherent spatially harmonic illumination can be used for new diffraction and imaging methods to study mesoscopic materials. A phase-contrast imaging technique is feasible whereby a sample is inserted into one of the beams while they are separated, as in the case of a classical interferometer. Any interaction with that beam will induce significant changes in the interference pattern, allowing the extraction of high-resolution information on the sample from the new phase pattern produced. A second technique would be moiré imaging whereby the sample is placed behind the bilens within the interference field. Standing-wave techniques are evident: a sample could be scanned across the periodic interference field and secondary processes (e.g., fluorescence, secondary electrons) would be detected by a detector placed to one side of the beam.

The bilens interferometer presented here exhibits major advantages over other interferometer schemes taken from classical optics such as Young double slits, Fresnel double mirrors, or bi-prisms [9-12]. Manufacturing of micro-slits, mirrors, and prisms for hard x-rays is a challenging technological task considering the requirements of surface and shape (edges) quality. In contrast, for silicon planar lenses, well-developed microelectronics technology is used, providing superior lens quality [4]. Furthermore, unlike slits, mirrors, and prisms, the bilens system can be used at high photon energies, up to 100 keV. The bilens system has the advantage over double slits as it focuses x-rays into the region where the two beams intersect, leading to an intensity gain factor for our nano-interferometer with respect to a hypothetical linear slit of 50 nm of at least 3 orders of magnitude.

In addition to imaging applications, the bilens interferometer could also be used for coherence diagnostics of optics and sources at existing synchrotrons. Silicon bilenses are stable under extremely powerful beams and relatively insensitive to mechanical vibrations. We expect that they will also be widely used for beam characterization for future free-electron x-ray laser sources.

ACKNOWLEDGMENTS

Authors are very grateful to T. Roth and C. Detlefs for their invaluable assistance at the ID06 ESRF beamline.

REFERENCES

1. A. Snigirev et al., *Nature* **384**, 49 (1996).
2. V. Aristov et al., *Appl. Phys. Lett.* **77**, 4058 (2000).
3. C. G. Schroer et al., *Appl. Phys. Lett.* **82**, 1485 (2003).
4. A. Snigirev et al., Proc. SPIE **6705**, 670506-1 (2007).
5. A. Snigirev et al., *Phys Rev Lett.* **103**, 064801 (2009).
6. A. Snigirev et al., to be published.
7. V. Kohn, I. Snigireva, and A. Snigirev, *Phys. Rev. Lett*. **85**, 2745 (2000).
8. U. Bonse and M. Hart, Appl. *Phys. Lett.* **6**, 155 (1965).
9. W. Leitenberger, S. M. Kuznetsov, and A. Snigirev, *Opt. Commun*. **191**, 91 (2001).
10. K. Fezzaa et al., *J. X-ray Science and Technology* **7**, 12 (1997).
11. A. R. Lang and A. P. Makepeace, *J. Synchrotron Radiat*. **6**, 59 (1999).
12. A. F. Isakovic et al., *J. Synchrotron Radiat*. **17**, 451 (2010).